analytical chemistry

pubs.acs.org/ac Letter

Glass Transition Temperatures of Individual Submicrometer Atmospheric Particles: Direct Measurement via Heated Atomic Force Microscopy Probe

Ziying Lei, Jing Zhang, Emily A. Mueller, Yao Xiao, Katherine R. Kolozsvari, Anne J. McNeil, Mark M. Banaszak Holl, and Andrew P. Ault*

Cite This: *Anal. Chem.* 2022, 94, 11973−11977 Read Online

ACCESS | Metrics & More | Article Recommendations | Supporting Information

ABSTRACT: The phase (solid, semisolid, or liquid) of atmospheric aerosols is central to their ability to take up water or undergo heterogeneous reactions. In recent years, the unexpected prevalence of viscous organic particles has been shown through field measurements and global atmospheric modeling. The aerosol phase has been predicted using glass transition temperatures (T_g), which were estimated based on molecular weight, oxygen:carbon ratio, and chemical formulae of organic species present in atmospheric particles via studies of bulk materials. However, at the most important sizes for cloud nucleation (~50−500 nm), particles are complex mixtures of numerous organic species, inorganic salts, and water with substantial particle-to-particle variability. To date, direct measurements of T_g have not been feasible for individual atmospheric particles. Herein, nanothermal analysis (NanoTA), which uses a resistively heated atomic force microscopy (AFM) probe, is combined with AFM photothermal infrared (AFM-PTIR) spectroscopy to determine the T_g and composition of individual particles down to 76 nm in diameter at ambient temperature and pressure. Laboratory-generated proxies for organic aerosol (sucrose, ouabain, raffinose, and maltoheptaose) had similar T_g values to bulk T_g values measured with differential scanning calorimetry (DSC) and the T_g predictions used in atmospheric models. Laboratory-generated phase-separated particles and ambient particles were analyzed with NanoTA + AFM-PTIR showing intraparticle variation in composition and T_g. These results demonstrate the potential for NanoTA + AFM-PTIR to increase our understanding of viscosity within submicrometer atmospheric particles with complex phases, morphologies, and compositions, which will enable improved modeling of aerosol impacts on clouds and climate.

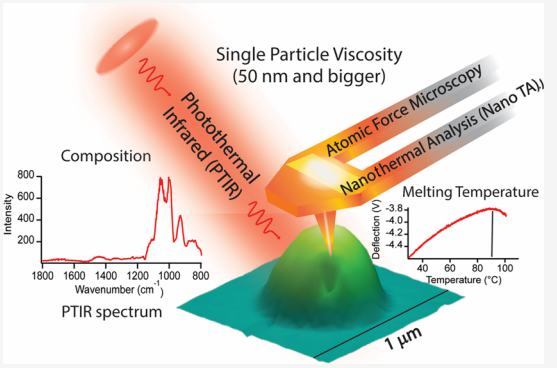

Organic species are ubiquitous within atmospheric aerosols and are both directly emitted to the atmosphere and formed secondarily through reactions that lower the vapor pressure of volatile species, causing them to condense on or react with existing aerosol transferring mass to the condensed phase. Individual particles can contain thousands of species in a single 100 nm particle, leading to a complex mixture of organic molecules, inorganic salts, and water.[1] Organic material is a significant component of atmospheric aerosols, accounting for greater than 50% of the mass of particulate matter less than 2.5 μm in diameter ($PM_{2.5}$).[2] These organic species play a central role in determining the impacts of atmospheric aerosols on climate, air quality, and human health by scattering solar radiation, nucleating cloud droplets, and depositing deep in the lungs.[1−3]

Traditionally, organic-containing atmospheric aerosols were assumed to be liquid, with a homogeneous mixture of water, organics, and salts. However, recent studies show that they are much more complex, with semisolid and solid organic phases observed,[4,5] as well as liquid−liquid phase separations.[6] Atmospheric observations measured the fraction of ambient solid organic particles bouncing off of smooth, hard surfaces and demonstrated solid particles at the key sizes for aerosol climate impacts (50−500 nm).[4,7] Laboratory studies of bulk materials used as proxies for atmospheric organic species showed viscosities (η) ranging from that of liquid water (10^{-3} Pa s) to glass marbles (>10^{12} Pa s) using differential scanning calorimetry (DSC).[8,9] High viscosities slow atmospheric chemical reactions as they decrease diffusion and mixing time scales within particles,[9,10] as predicted by the Stokes−Einstein equation for particles with viscosities from 10^{-3} to 10^{12} Pa s.[11,12] Direct measurements were developed to confirm

Received: May 6, 2022
Accepted: August 17, 2022
Published: August 22, 2022

https://doi.org/10.1021/acs.analchem.2c01979
Anal. Chem. 2022, 94, 11973−11977

these predictions, including the poke-and-flow technique ($10 < \eta < 10^6$ Pa s)[11] and bead-mobility method ($10^{-3} < \eta < 10^3$ Pa S) for large droplets (>30 μm).[13] Further approaches have included particle coalescence in aerosol optical tweezers[14] and broadband dielectric spectroscopy.[15] However, these methods have been limited to larger particles, films, or bulk materials and are not able to probe individual particles at the sizes of typical organic aerosol in the atmosphere (mode ~100 nm).[3] Thus, methods are needed to probe viscosities in individual submicrometer atmospheric particles.

Glass transition temperature (T_g) is a frequently used parameter to describe phase states,[8] representing a non-equilibrium phase transition from a liquid or semisolid state to a glassy solid state when the temperature decreases. Atomic force microscopy (AFM) has been used to monitor surface tension and probe phase through indentation using force curves,[16,17] but without chemical information, understanding complex atmospheric particles can be challenging. Atmospheric models attempting to predict organic aerosol phase states as a function of chemical composition have used the T_g of available proxies for organic aerosols to predict T_g based on molecular weight (MW) or elemental formulae ($C_xH_yO_z$).[18] Models of organic aerosol phases predict that particles are mostly liquid or semisolid in the planetary boundary layer,[19,20] but examples of unexpectedly semisolid[21] and solid[22] aerosols continue to be observed. Thus, new approaches are needed to directly measure T_g and composition at important sizes for the atmosphere (<1 μm).

As impacted particles spread leading to a larger projected area diameter, the volume of individual particles was obtained via SPIP 6.2.6 software (Image Metrology, Hørsholm, Denmark) to determine the volume equivalent diameter (D_{ve}), which can be related to the more atmospherically relevant aerodynamic diameter (d_a). Herein, we use nanothermal analysis (NanoTA) to determine the T_g of individual particles down to less than 100 nm (volume equivalent diameter). Directly measuring the melting temperature (T_m) and converting to T_g via the Boyer−Beaman rule[23] has been used to determine the T_g of many organic materials (not all will have a T_g). NanoTA uses a resistively heated AFM probe,[24] and deflection (Figure 1a) is monitored during a controlled temperature ramp. Sucrose, a common proxy for viscous organics in the atmosphere,[9] was aerosolized and inertially impacted onto silicon wafers using a microanalysis particle sampler (MPS-3, California Measurements, Inc.) on the smallest stage with a size cut at d_a = 400 nm.[25] At the T_m, the particle melts sufficiently for the probe to sink in creating an indentation (Figure 1b). The thermal analysis was combined with chemical information using AFM photothermal infrared (PTIR) spectroscopy. AFM-PTIR can obtain IR spectra for particles less than 100 nm,[26,27] as shown for sucrose (Figure 1c). IR vibrational modes observed include ν(C−C) at 929 cm^{-1}, ν(C−O) at 997 cm^{-1}, 1055 and 1111 cm^{-1}, and δ(C−O−H) at 1437 cm^{-1}, similar to traditional IR spectra for sucrose.[26,28,29]

The NanoIR3 system integrated with a nanothermal analysis (NanoTA) module (Bruker, Santa Barbara, CA) was operated in contact mode for thermal analysis. The resistively heated thermal probes (20−30 nm tip) (VITA-HE-NANOTA-200; ThermaLever AN2−300, Bruker) were calibrated before each session using three polymeric materials with sharp melting points: polycaprolactone (PCL, T_m = 55 °C), high-density polyethylene (HDPE, T_m = 116 °C), and polyethylene

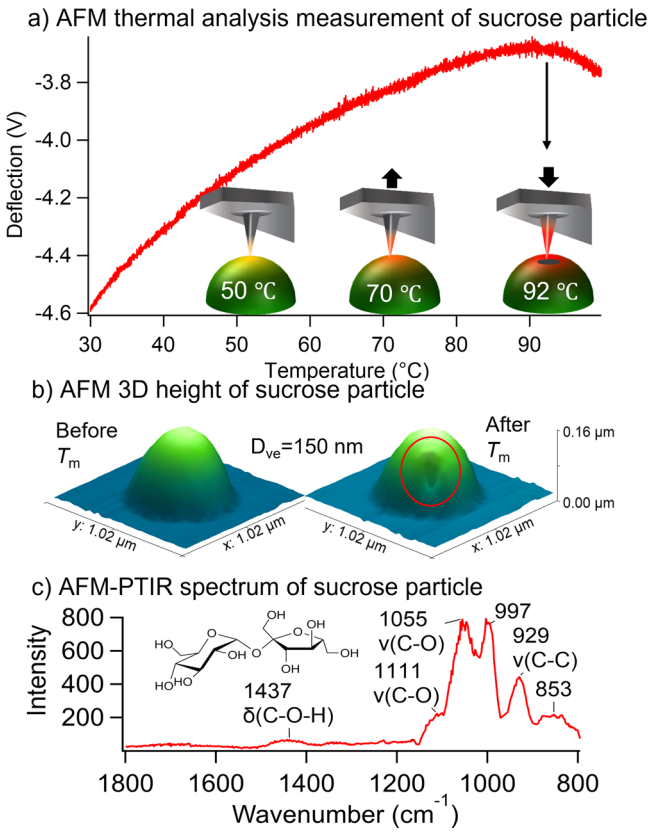

Figure 1. (a) Deflection of nanothermal analysis(NanoTA) atomic force microscopy (AFM) probe during a temperature ramp and cartoon depicting probe deflection at different temperatures for an individual sucrose particle approaching the melting temperature (T_m). (b) AFM 3D height image of representative submicrometer sucrose particle before and after NanoTA analysis (volume equivalent diameter, d_{ve}, 150 nm); the red circle represents the location where the thermal probe melted the particle. (c) Averaged PTIR spectrum of submicrometer individual sucrose particles. Molecule was drawn in ChemDraw.

terephthalate (PET, T_m = 235 °C) (Figure S1). Details about aerosol generation, DSC measurements with temperature ramp (Figure S2), chemical characterization, and the T_g model are available in the Supporting Information.

To confirm the ability of NanoTA to probe multiple compounds representative of viscous organic species in the atmosphere, sucrose, ouabain, raffinose, and maltoheptaose were aerosolized and impacted. Particles between 76−611 nm were analyzed (Figure 2a), which cover a key size range for organic particles in the atmosphere. The average T_m values are shown in Figure 2b and are converted to T_g, which agree with previous studies.[5,8,30] Individual temperature ramps for single particles are shown in Figure S3. Similar melting temperatures were observed for ouabain and raffinose particles (140 and 143 °C, respectively), which have similar molecular weights (584 and 594.5 g/mol, respectively). To compare with more traditional methods for determining T_g, aerosolized samples were also collected and analyzed for T_m (and converted to T_g) using DSC (model Q2000, equipped with a RCS90 accessory, TA Instruments) (Figure 2c). Ouabain, raffinose, and maltoheptaose DSC results were within uncertainty of the NanoTA results, while NanoTA of sucrose was slightly lower. This indicates differences between the particles analyzed by NanoTA and the DSC sample consisting of wet aerosol

https://doi.org/10.1021/acs.analchem.2c01979
Anal. Chem. 2022, 94, 11973−11977

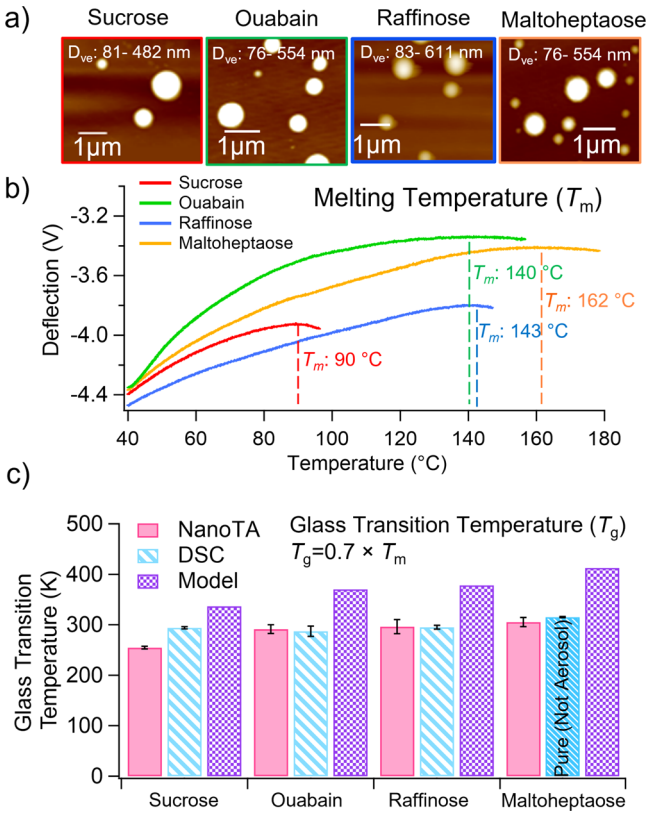

Figure 2. (a) AFM height images of submicrometer sucrose, ouabain, raffinose, and maltoheptaose particles. (b) Average melting temperature of 20 individual particles from AFM thermal analysis measurements. (c) Glass transition temperature of sucrose, ouabain, raffinose, and maltoheptaose measured by NanoTA, DSC, and model calculation. Maltoheptaose T_g was measured for a pure powder by DSC (not an aerosolized and impacted sample).

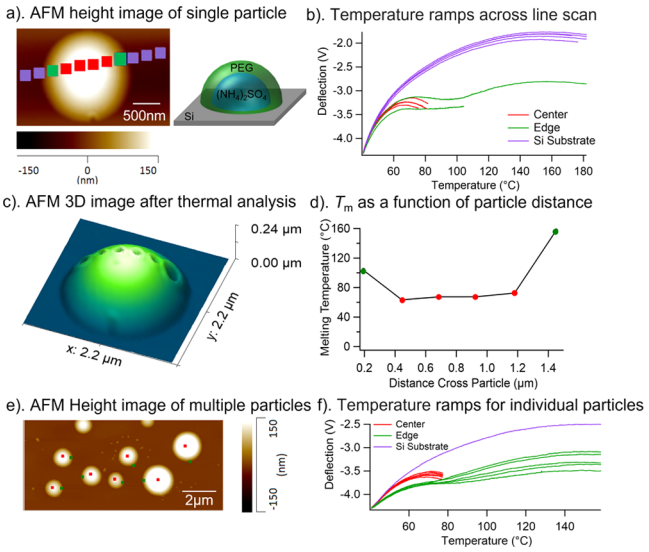

Figure 3. (a) AFM height image of PEG/AS particles with line scan; each marker represents the location of where a T ramp was collected. The different colors represent the center(red) and edge (green) of the particle and substrate (purple). (b). Individual T ramps of the line scan correspond to (a). (c) AFM 3D image of the same particle after NanoTA analysis. (d) T_m as a function of particle distance. (e) AFM height image of multiple PEG/AS particles; color dots represent the locations of where T ramps were collected. (f) T ramps of particles in (e). Note that for (c) the z axis length is different than the x and y axes lengths to improve visualization.

collected on the DSC pan (3 mg required). The difference was likely due to water trapped within the drying sucrose particles prior to recrystallization,[31] which was observed in the DSC at 100 °C, as well as via a ν(OH) stretch of the PTIR spectrum, or changes in morphology.[32] For maltoheptaose, DSC could not obtain a T_m for aerosolized particles, also due to water. Thus, pure maltoheptaose powder was analyzed via DSC, of the type used to generate the maltoheptaose particles analyzed by NanoTA. Water is a plasticizer, and its presence changes the viscosity of aerosols. This plasticization represents a challenge for using DSC to analyze aerosols and highlights the beneficial ability of NanoTA to directly probe water-containing particles as a significant strength. The NanoTA results were also compared with modeled T_g using the approach described in DeRieux et al.,[33] which predicts CH and CHO compounds using the number of different C, H, and O atoms. The estimated T_g from the model are higher than the measurements, suggesting that there are significant differences of T_g between bulk material and individual aerosol particles.

In the atmosphere, particles are frequently not homogeneous and have more complex morphologies (i.e., core−shell or partially engulfed). NanoTA was used to examine particles with ammonium sulfate cores and polyethylene glycol (PEG) shells. A height map was obtained (Figure 3a), which was collected in contact mode, and the PEG acts as a thick coating over the ammonium, as shown by the cartoon in Figure 3a and observed previously.[34] A NanoTA line scan was performed with temperature ramps collected at 0.3 μm steps across the PEG-coated particle (Figure 3b). The holes caused by the AFM heating probe in the PEG after the line scan are shown in Figure 3c. The T_m obtained at each point of the line scan demonstrates that the thermal probe was able to fully penetrate the PEG and reach the silicon on the edge of the particle with 146 nm thickness, but it was not able to melt through to the core due to the thick coating in the center of the particle. (Figure 3d). To explore the reproducibility of the method and the ability to probe smaller aerosol sizes, multiple individual particles with D_{ve} 80−300 nm were imaged (Figure 3e) and analyzed by NanoTA (Figure 3f). T_m ramps were conducted at the center and edge of individual particles. Representative PTIR spectra of the edge and core were collected to confirm the PEG layer (Figure S4), and our results suggests that the NanoTA probe deflection maxima correspond to melting the shell. This results in similar melting temperatures for the edge and center of 70 °C, corresponding to the T_g of PEG. At the edge of the particle, the thermal probe melted the PEG and reached the silicon substrate at 80 °C and turned over again at 160 °C (similar to the substrate). PTIR spectral maps were collected at 930 cm^{-1} to identify PEG and at 1400 cm^{-1} for the $\delta(NH_4^+)$ of ammonium sulfate, which show different spatial distributions of chemical compositions (Figure S5) but highlight PEG covering the entire particle.

To demonstrate that this method can be applied to complex atmospheric particles, individual ambient particles were collected and analyzed with NanoTA for the first time. Particle sizes ranged from 76−186 nm (D_{ve}), and core−shell morphologies of ambient particles were observed through a combination of height (Figure 4a) and deflection (Figure 4b) images. Both temperature ramps and PTIR spectra were collected to determine the T_g of the particles and to

https://doi.org/10.1021/acs.analchem.2c01979
Anal. Chem. 2022, 94, 11973−11977

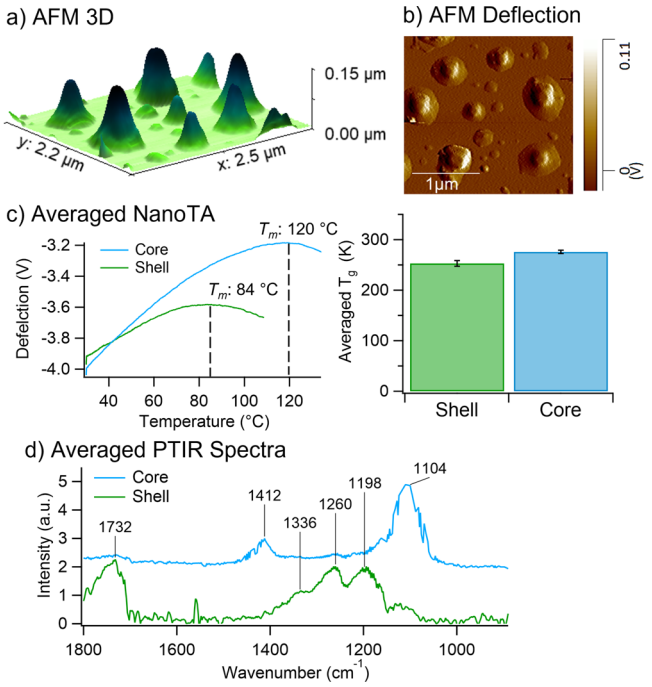

Figure 4. (a) AFM 3D image of ambient particles. (b). AFM deflection image. (c) T_m ramp for particle core (blue) and shell (green). (d) AFM-PTIR spectra of particle core (blue) and shell (green).

understand their chemical compositions (Figure 4c, d). Distinct melting temperatures showed that the shell had a relatively lower T_m at 84 °C and the particle core was 120 °C (Figure 4c). This result illustrates that the organic shell is more likely to be in the liquid or semisolid phase, and the core is more likely to be in a solid phase (likely dried between collection and analysis). Modes at 1104 and 1412 cm^{-1} in the particle core represent $\nu_{as}(SO_4^{2-})$ and $\delta(NH_4^+)$,[26] respectively, indicative of ammonium sulfate, which is common in atmospheric particles. The T_m values of ammonium bisulfate particles were measured, which is similar to the temperature we observed for the ammonium sulfate core of ambient particles (Figure S6). For the shell, modes at 1336 and 1732 cm^{-1} were assigned to δ(C−H) and ν(C═O), respectively,[28] which suggest organic compounds in the shell. The combined chemical information and T_g measurements on authentic submicrometer ambient particles show the potential to study atmospheric particles with complex physicochemical properties.

The application of nanoscale thermal analysis to submicrometer solid and semisolid particles is an important measurement science advancement for aerosol particle analysis. This capability is particularly needed for viscous and solid ultrafine (<100 nm) and accumulation mode (100−1000 nm) aerosols, which are being observed in unexpected locations, including exhaled virus-containing particles in indoor environments,[21] along the humid coastline of the Alaskan Arctic,[22] and in midlatitude regions.[4,7] The detailed analyses of well-characterized proxies for viscous organic aerosol (e.g., sucrose) and comparison with DSC and model-predicted T_g values demonstrate the potential of NanoTA. T_g from measurements combined with PTIR spectra[26] will provide a key experimental constraint, as predictions of organic species viscosities have not previously been constrained in atmospheric models. NanoTA was applied to study submicrometer single-component model systems, phase-separated particles, and ambient aerosol particles for the first time. By obtaining particle size, morphology, phase, chemical composition, and melting temperature simultaneously, NanoTA + AFM-PTIR will advance our understanding of aerosol particles with broad impacts on global climate and human health.

■ ASSOCIATED CONTENT

Supporting Information

The Supporting Information is available free of charge at https://pubs.acs.org/doi/10.1021/acs.analchem.2c01979.

Additional experimental details, DSC bulk measurement, AFM thermal analysis calibration, PTIR analysis, T_g model, individual temperature ramps for submicrometer particles from proxies, PTIR spectra for phase-separated particles, and T_m values for ammonium bisulfate particles (PDF)

■ AUTHOR INFORMATION

Corresponding Author

Andrew P. Ault − *Department of Chemistry, University of Michigan, Ann Arbor, Michigan 48109, United States;* orcid.org/0000-0002-7313-8559; Email: aulta@umich.edu

Authors

Ziying Lei − *Department of Environmental Health Sciences, University of Michigan, Ann Arbor, Michigan 48109, United States;* orcid.org/0000-0003-3071-0698

Jing Zhang − *Department of Chemical and Biological Engineering, Monash University, Melbourne, Victoria 3800, Australia*

Emily A. Mueller − *Department of Chemistry, University of Michigan, Ann Arbor, Michigan 48109, United States*

Yao Xiao − *Department of Chemistry, University of Michigan, Ann Arbor, Michigan 48109, United States;* orcid.org/0000-0003-3661-2845

Katherine R. Kolozsvari − *Department of Chemistry, University of Michigan, Ann Arbor, Michigan 48109, United States*

Anne J. McNeil − *Department of Chemistry, University of Michigan, Ann Arbor, Michigan 48109, United States; Macromolecular Science and Engineering Program, University of Michigan, Ann Arbor, Michigan 48109-2800, United States;* orcid.org/0000-0003-4591-3308

Mark M. Banaszak Holl − *Department of Chemical and Biological Engineering, Monash University, Melbourne, Victoria 3800, Australia;* orcid.org/0000-0001-7759-7456

Complete contact information is available at: https://pubs.acs.org/10.1021/acs.analchem.2c01979

Author Contributions

Ziying Lei and Jing Zhang contributed equally to this work.

Notes

The authors declare no competing financial interest.

■ ACKNOWLEDGMENTS

The authors acknowledge funding by the National Science Foundation (NSF) through CAREER award CHE-1654149

(Ault). E.A.M acknowledges funding from NSF award CHE-1955000.

REFERENCES

(1) Riemer, N.; Ault, A. P.; West, M.; Craig, R. L.; Curtis, J. H. *Rev. Geophys.* **2019**, *57* (2), 187−249.
(2) Jimenez, J. L.; Canagaratna, M. R.; Donahue, N. M.; Prevot, A. S. H.; Zhang, Q.; Kroll, J. H.; DeCarlo, P. F.; Allan, J. D.; Coe, H.; Ng, N. L.; et al. *Science* **2009**, *326* (5959), 1525−1529.
(3) Pöschl, U. *Angew. Chem.-Int. Ed.* **2005**, *44* (46), 7520−7540.
(4) Slade, J. H.; Ault, A. P.; Bui, A. T.; Ditto, J. C.; Lei, Z.; Bondy, A. L.; Olson, N. E.; Cook, R. D.; Desrochers, S. J.; Harvey, R. M.; Erickson, M. H.; Wallace, H. W.; Alvarez, S. L.; Flynn, J. H.; Boor, B. E.; Petrucci, G. A.; Gentner, D. R.; Griffin, R. J.; Shepson, P. B. *Environ. Sci. Technol.* **2019**, *53*, 4977.
(5) Zobrist, B.; Marcolli, C.; Pedernera, D. A.; Koop, T. *Atmos. Chem. Phys.* **2008**, *8* (17), 5221−5244.
(6) You, Y.; Renbaum-Wolff, L.; Carreras-Sospedra, M.; Hanna, S. J.; Hiranuma, N.; Kamal, S.; Smith, M. L.; Zhang, X.; Weber, R. J.; Shilling, J. E.; et al. *Proc. Natl. Acad. Sci. U. S. A.* **2012**, *109* (33), 13188−13193.
(7) Virtanen, A.; Joutsensaari, J.; Koop, T.; Kannosto, J.; Yli-Pirila, P.; Leskinen, J.; Makela, J. M.; Holopainen, J. K.; Poeschl, U.; Kulmala, M.; et al. *Nature* **2010**, *467* (7317), 824−827.
(8) Koop, T.; Bookhold, J.; Shiraiwa, M.; Poschl, U. *Phys. Chem. Chem. Phys.* **2011**, *13* (43), 19238−19255.
(9) Reid, J. P.; Bertram, A. K.; Topping, D. O.; Laskin, A.; Martin, S. T.; Petters, M. D.; Pope, F. D.; Rovelli, G. *Nat. Commun.* **2018**, *9* (1), 956.
(10) Davies, J. F.; Wilson, K. R. *Chem. Sci.* **2015**, *6* (12), 7020−7027.
(11) Shiraiwa, M.; Ammann, M.; Koop, T.; Poschl, U. *Proc. Natl. Acad. Sci. U. S. A.* **2011**, *108* (27), 11003−11008.
(12) Evoy, E.; Maclean, A. M.; Rovelli, G.; Li, Y.; Tsimpidi, A. P.; Karydis, V. A.; Kamal, S.; Lelieveld, J.; Shiraiwa, M.; Reid, J. P.; et al. *Atmos. Chem. Phys.* **2019**, *19* (15), 10073−10085.
(13) Renbaum-Wolff, L.; Grayson, J. W.; Bertram, A. K. *Atmos. Chem. Phys.* **2013**, *13* (2), 791−802.
(14) Bzdek, B. R.; Power, R. M.; Simpson, S. H.; Reid, J. P.; Royall, C. P. *Chem. Sci.* **2016**, *7* (1), 274−285.
(15) Zhang, Y.; Katira, S.; Lee, A.; Lambe, A. T.; Onasch, T. B.; Xu, W.; Brooks, W. A.; Canagaratna, M. R.; Freedman, A.; Jayne, J. T.; et al. *Atmos. Meas. Technol.* **2018**, *11* (6), 3479−3490.
(16) Lee, H. D.; Ray, K. K.; Tivanski, A. V. *Anal. Chem.* **2017**, *89* (23), 12720−12726.
(17) Ray, K. K.; Lee, H. D.; Gutierrez, M. A.; Chang, F. J.; Tivanski, A. V. *Anal. Chem.* **2019**, *91* (12), 7621−7630.
(18) DeRieux, W. S. W.; Li, Y.; Lin, P.; Laskin, J.; Laskin, A.; Bertram, A. K.; Nizkorodov, S. A.; Shiraiwa, M. *Atmos. Chem. Phys.* **2018**, *18* (9), 6331−6351.
(19) Shiraiwa, M.; Li, Y.; Tsimpidi, A. P.; Karydis, V. A.; Berkemeier, T.; Pandis, S. N.; Lelieveld, J.; Koop, T.; Pöschl, U. *Nat. Commun.* **2017**, *8*, 15002.
(20) Shiraiwa, M.; Zuend, A.; Bertram, A. K.; Seinfeld, J. H. *Phys. Chem. Chem. Phys.* **2013**, *15* (27), 11441−11453.
(21) Huynh, E.; Olinger, A.; Woolley, D.; Kohli, R. K.; Choczynski, J. M.; Davies, J. F.; Lin, K.; Marr, L. C.; Davis, R. D. *Proc. Natl. Acad. Sci. U. S. A.* **2022**, *119* (4), e2109750119.
(22) Kirpes, R. M.; Lei, Z.; Fraund, M.; Gunsch, M. J.; May, N. W.; Barrett, T. E.; Moffett, C. E.; Schauer, A. J.; Alexander, B.; Upchurch, L. M.; China, S.; Quinn, P. K.; Moffet, R. C.; Laskin, A.; Sheesley, R. J.; Pratt, K. A.; Ault, A. P. *Proc. Natl. Acad. Sci. U. S. A.* **2022**, *119* (14), e2104496119.
(23) Beaman, R. G. *J. Polym. Sci.* **1952**, *9* (5), 470−472.
(24) Hammiche, A.; Reading, M.; Pollock, H.; Song, M.; Hourston, D. *Rev. Sci. Instrum.* **1996**, *67* (12), 4268−4274.
(25) Lei, Z.; Olson, N. E.; Zhang, Y.; Chen, Y.; Lambe, A. T.; Zhang, J.; White, N. J.; Atkin, J. M.; Banaszak Holl, M. M.; Zhang, Z.; Gold, A.; Surratt, J. D.; Ault, A. P. *ACS Earth Space Chem.* **2022**, *6*, 871.
(26) Bondy, A. L.; Kirpes, R. M.; Merzel, R. L.; Pratt, K. A.; Banaszak Holl, M. M.; Ault, A. P. *Anal. Chem.* **2017**, *89* (17), 8594−8598.
(27) Or, V. W.; Estillore, A.; Grassian, V.; Tivanski, A. V. *Analyst* **2018**, *143* (12), 2765−2774.
(28) Olson, N. E.; Xiao, Y.; Lei, Z.; Ault, A. P. *Anal. Chem.* **2020**, *92*, 9932.
(29) Brizuela, A. B.; Bichara, L. C.; Romano, E.; Yurquina, A.; Locatelli, S.; Brandan, S. A. *Carbohydr. Res.* **2012**, *361*, 212−218.
(30) Slade, L.; Levine, H. *J. Food Eng.* **1995**, *24* (4), 431−509.
(31) Drake, A. C.; Lee, Y.; Burgess, E. M.; Karlsson, J. O. M.; Eroglu, A.; Higgins, A. Z. *PLoS One* **2018**, *13* (1), e0190713.
(32) Kalika, D.; Gibson, D.; Quiram, D.; Register, R. A. *J. Polym. Sci., Part B: Polym. Phys.* **1998**, *36* (1), 65−73.
(33) DeRieux, W.-S. W.; Li, Y.; Lin, P.; Laskin, J.; Laskin, A.; Bertram, A. K.; Nizkorodov, S. A.; Shiraiwa, M. *Atmos. Chem. Phys.* **2018**, *18* (9), 6331−6351.
(34) O'Brien, R. E.; Wang, B.; Kelly, S. T.; Lundt, N.; You, Y.; Bertram, A. K.; Leone, S. R.; Laskin, A.; Gilles, M. K. *Environ. Sci. Technol.* **2015**, *49* (8), 4995−5002.

https://doi.org/10.1021/acs.analchem.2c01979
Anal. Chem. 2022, 94, 11973−11977